

Wind-Driven Radial-Engine-Shaped Triboelectric Nanogenerators for Self-Powered Absorption and Degradation of NO_x

Kai Han, Jianjun Luo, Yawei Feng, Qingsong Lai, Yu Bai, Wei Tang,* and Zhong Lin Wang*

Cite This: <https://dx.doi.org/10.1021/acsnano.9b08496>

Read Online

ACCESS |

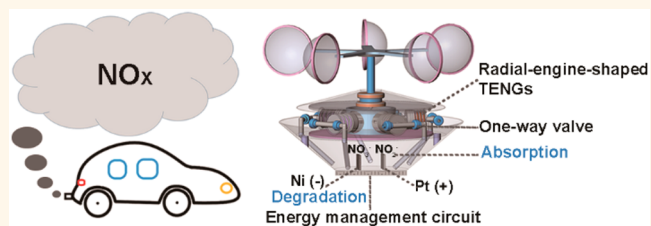
Metrics & More

Article Recommendations

Supporting Information

ABSTRACT: As one of the major air pollutants, NO_x is rather challenging to remove. The main treatment method is catalytic reduction with plenty of reducing agents, which lacks any effective control in an open air environment such as urban spaces. It is necessary to seek a self-powered electrochemical process for environmental treatment. The triboelectric nanogenerator (TENG), a developing technology with various advantages, is widely used in energy and environmental monitoring and cleaning. In this work, a radial-engine-shaped TENG system with five stacked TENGs is designed to synchronously absorb NO_x and degrade its main enrichment forms of nitrate and nitrite in aqueous solution. In addition, the system possesses inherent phase differences and outputs continuous direct current after rectification. Moreover, we demonstrated that, driven by artificial wind at a speed of 6 m/s, the NO_x generated by a chemical method was effectively degraded by the radial-engine-shaped TENG system.

KEYWORDS: triboelectric nanogenerators, self-powered, NO_x, electrocatalytic, radial engine



With the consumption of fossil fuels, various contaminants and exhaust gases are generated during combustion and released into the air.^{1–5} Among these pollutants, NO_x is a tricky object with huge harm both to the environment and to human beings. As a major source of acid rain, the damage to crops and other plants is incalculable.^{5–7} In addition, it can irritate the respiratory tract and may cause chronic diseases.^{8–11} To control it within an acceptable low toxicity range, catalytic reduction is the main treatment method. However, such a catalytic method focuses more on the sources of pollution with plenty of reducing agents such as ammonia and urea,^{5,12–15} which is not feasible for the open air. Moreover, due to the poor solubility of NO_x, researchers have made much effort such as pressurization and high capture performance materials to enhance their absorption of trace NO_x.^{16–18} These inevitably increase requirements for equipment and materials. Thus, other appropriate ways to control NO_x pollution are required. Once the chemical equilibrium is broken by degradation of the reaction products between NO_x and water, the absorption and abatement of NO_x can continue. It is necessary to seek a self-powered electrochemical process for effective removal of such pollutants.

The triboelectric nanogenerator (TENG), a developing technology in energy harvesting, is widely used since its invention in 2012.¹⁹ Originating from Maxwell displacement

current, environmental mechanical energy can be converted into electric energy by different kinds of TENGs based on four basic working modes.^{20,21} It possesses advantages of simple fabrication, a wide range of material sources, and low-frequency adaptability and has been widely applied in numerous fields.^{22–30} In the open air, wind energy is much easier to obtain and is clean enough as a natural power source to realize a series of self-powered applications such as sensing and pollutant degradation.^{31–36} Therefore, the TENG is very suitable for NO_x pollution removal in open air conditions. To enhance the degradation performance, the piston motion is utilized to lead the gas flow and help achieve the absorption of NO_x into water.

In this work, a self-powered NO_x absorption and degradation system is designed, which consists of radial-engine-shaped TENGs, one-way valves, and an electrocatalytic system. Making use of one-way valves and piston movements, the NO_x can be inlet into water with the main enrichment forms of nitrate and nitrite. Considering the catalytic activity and corrosion resistance,^{37–40} Ni foam, with a large surface

Received: October 27, 2019

Accepted: February 7, 2020

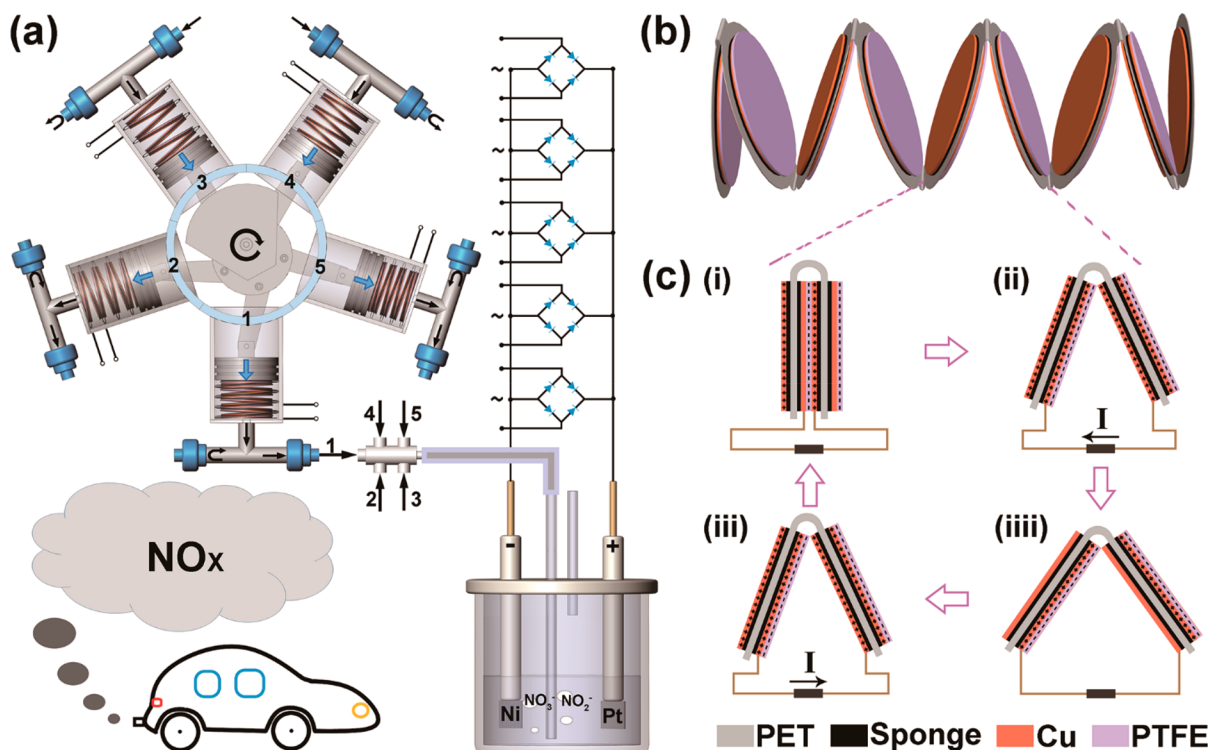


Figure 1. Schematic diagram and working principle. (a) NO_x absorption and degradation system. (b) Stacked TENGs. (c) Working principle of the TENG.

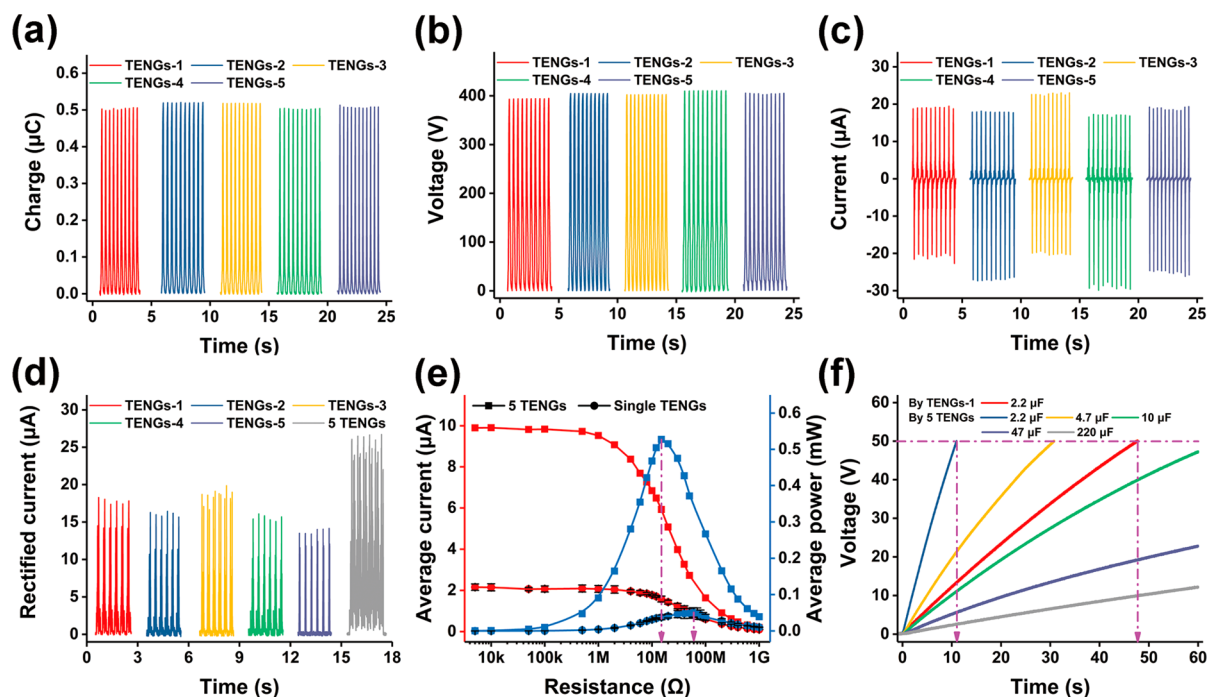


Figure 2. Basic performance of the radial-engine-shaped TENGs at a rotation frequency of 3 Hz. (a) Transferred charge. (b) Open-circuit voltage. (c) Short-circuit current. (d) Rectified short-circuit current. (e) Average rectified current and average power with different external resistances. (f) Charging performance with different capacitors.

area, is chosen as catalyst and working electrode (WE). Driven by wind, the system can synchronously realize the absorption and electrocatalytic degradation of NO_x in an aqueous solution. In addition, due to the advantage of phase position of the five chambers, the radial-engine-shaped TENGs output continuous direct current (DC) after rectification.⁴¹

RESULTS AND DISCUSSION

Figure 1a shows a schematic diagram of the NO_x absorption and degradation system. A radial engine structure is utilized for TENGs, in which five gas chambers are assembled in a plane with the number from 1 to 5. To well control the air flow, two one-way valves are coordinately connected with each gas

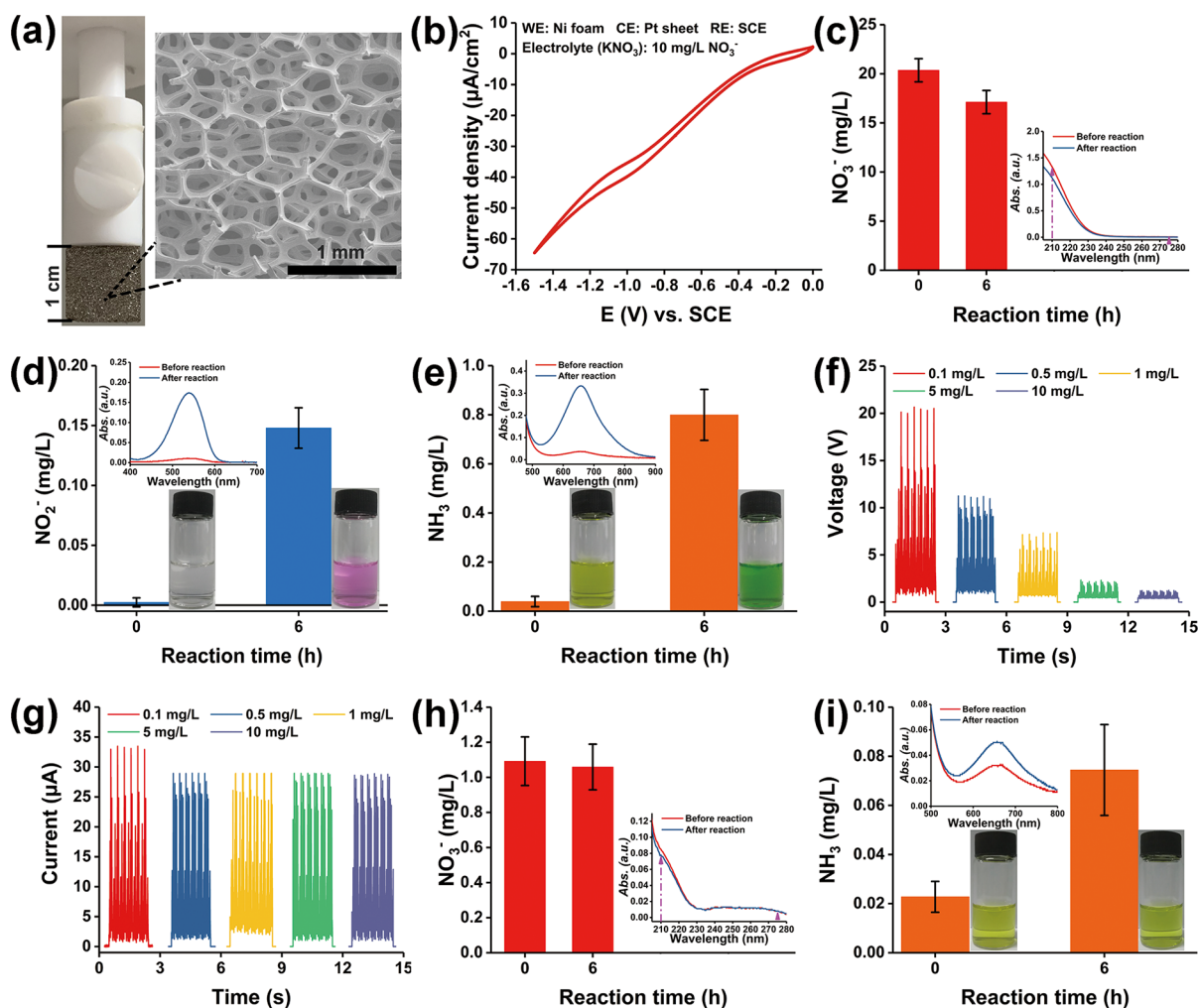


Figure 3. Degradation of NO_3^- . (a) Photograph of the working electrode and a SEM picture of the Ni foam. (b) CV curve in a 10 mg/L NO_3^- solution. (c) Concentration variation of NO_3^- and (d) NO_2^- and (e) NH_3 after a 6 h degradation of 20 mg/L NO_3^- with 0.1 mol/L K_2SO_4 by DC power at -3 V. (f) Voltage and (g) current data between two electrodes in different concentrations of NO_3^- solutions by the radial-engine-shaped TENGs after rectification. (h) Concentration variation of NO_3^- and (i) NH_3 after 6 h of degradation of 1 mg/L NO_3^- by the radial-engine-shaped TENGs after rectification.

chamber. The black rotation arrow stands for the rotation direction under the external driving force for the self-powered system. When a full turn is over, all five pistons complete a period of movement. The blue arrows show the different motion state in these chambers at the same time. Figure S1a shows the pull and push process in a single chamber during piston motion. A six-way valve is used to gather the gas from different chambers. The black arrows show the directions of flows. With the help of one-way valves, the gas containing NO_x from the open air is transformed into the water and washed continuously, leaving soluble harmful substances as nitrate and nitrite. Five rectifiers are connected with each TENG to get continuous DC power to degrade these substances. More details about reaction products during the absorption and electrocatalytic degradation process are illustrated in Figure S1b. Figure S2a shows a three-dimensional diagram of the radial-engine-shaped TENGs. The schematic fabrication process of the key actuating device is shown in Figure S2b. In each chamber, the piston is driven to do linear motion. Thus, a contact–separation mode TENG is selected. Considering that the motion displacement is long enough and the catalytic system needs sufficient power to degrade

contaminants, a stacked structure with eight TENGs in parallel is used (Figure 1b). Figure S3 shows the fabrication process of the stacked TENGs. PTFE and Cu films are chosen as triboelectricity materials, and PET is chosen as the substrate material to support other parts and ensure continuous bending. Both ends of the stacked TENGs are stuck to the piston and the chamber separately. As the piston moves, an electric signal is generated by the stacked TENGs. Figure 1c shows the working principle of the TENG. When the two films with different triboelectricity materials are separated, the potential on the Cu film side will drive the flow of charges to the other electrode and generate current through an external circuit. Inversely, when they are approaching each other, the potential built by the redistributed charges will drive charges to flow back to the Cu film and generate an inverse current.

After assembling the radial-engine-shaped TENGs, the basic performance is tested by an electrometer. Figure S4 shows a photograph of the top view of the radial-engine-shaped TENGs and the air flow control device. It should be noted that five position control baffles are set at the air outlet end of chambers to finely adjust their positions. Thanks to these, the

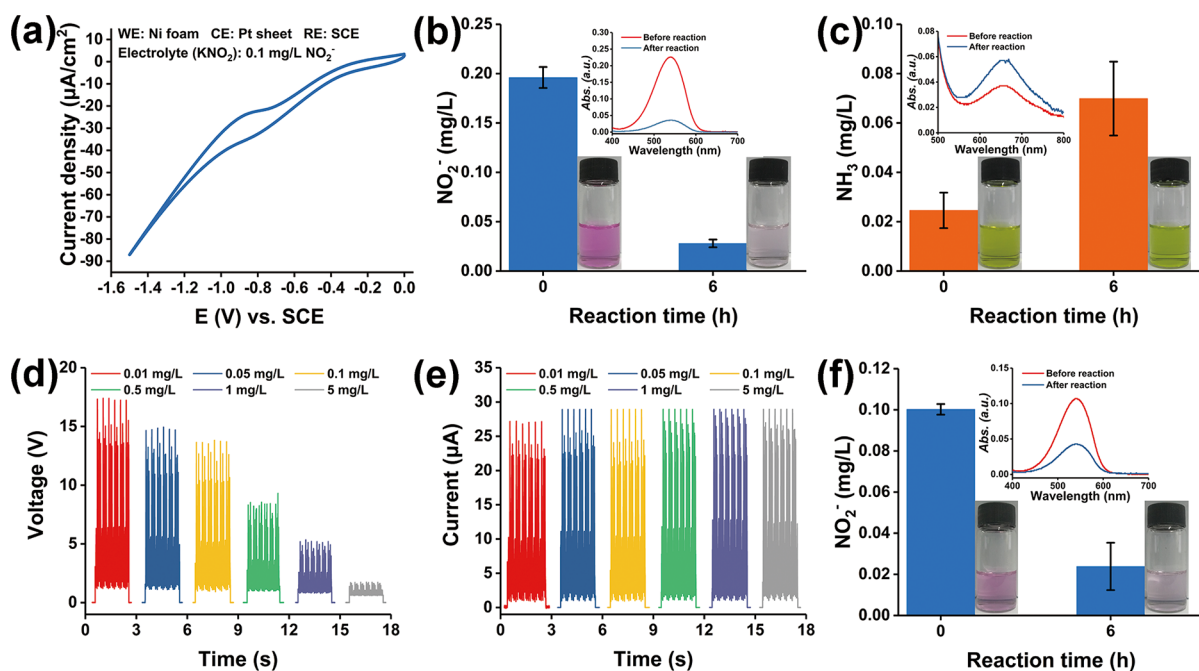


Figure 4. Degradation of NO_2^- . (a) CV curve in 1 mg/L NO_2^- solution. (b) Concentration variation of NO_2^- and (c) NH_3 after 6 h degradation of 0.2 mg/L NO_2^- with 0.1 mol/L K_2SO_4 by a DC power at -3 V. (d) Voltage and (e) current data between two electrodes in different concentrations of NO_2^- solutions by the radial-engine-shaped TENGs after rectification. (f) Concentration variation of NO_2^- after a 6 h degradation of 0.1 mg/L NO_2^- by the radial-engine-shaped TENGs after rectification.

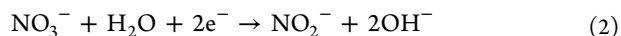
piston can keep the stacked TENGs having sufficient and vertical contact–separation motions. As shown in Figure 2a–c, there are no significant differences among five stacked TENGs at the rotation frequency of 3 Hz. The transferred charge reaches about $0.5 \mu\text{C}$, open-circuit voltage is around 400 V, and short-circuit current is about $20 \mu\text{A}$. Since these TENGs are used to drive the electrocatalytic reaction, power management with rectification is necessary. Apart from the measurement of each single stacked TENGs, the results by their parallel connection after rectification are also shown in Figure 2d. There are still no obvious differences among these single stacked TENGs. As a comparison, five stacked TENGs in parallel output higher peak currents. Moreover, since the five TENGs work alternatively, the current value always remains bigger than zero, showing a continuous DC output. This means a larger effective current and power,^{41,42} which is more suitable for an electrochemical reaction system. As shown in Figure 2e, the maximum average current value of five stacked TENGs is about 4.76 times that of single stacked TENGs. The maximum matched average power by five stacked TENGs is 0.53 mW with an external resistance of 15 M Ω . As for the single one, the maximum average power is 0.05 mW with the matched resistance of 60 M Ω . The detailed multiples data are illustrated in Figure S5, indicating that taking advantage of shifted phase, more than 5 times average power can be achieved at the same external resistance in the range of 0–300 M Ω . Furthermore, the charging performance is tested as well (Figure 2f). The single stacked TENG takes 4.6 times as long as five TENGs do to charge a 2.2 μF capacitor to a voltage of 50 V, and the charging time becomes longer with the capacitance increasing.

Since the main existing forms of NO_x in aqueous solution are nitrate and nitrite, the reaction process is simply expressed as below.



Therefore, KNO_3 and KNO_2 are used as the simulation contaminants. An electrocatalytic system with Ni as working electrode and Pt as counter electrode (CE) is introduced to conduct degradation experiments. In order to enhance catalytic effects, 99.9% pure Ni foam, which has a high surface area, is used. Figure 3a shows a photograph of a working electrode and a SEM picture of the Ni foam. To verify the catalytic degradation of nitrate, the cyclic voltammetry (CV) curve is measured in 10 mg/L NO_3^- solution with the reference of a saturated calomel electrode (SCE). The typical redox peaks can be easily distinguished in Figure 3b.^{39,43} To quantitatively detect the concentration of NO_3^- , the standard calibration curve is made by utilizing its specific absorption in the ultraviolet region (Figure S6a,b). In simulation degradation experiments, a 20 mg/L NO_3^- solution, which is within determination limit, is used as a pollutant source. Besides, with the purpose of speeding up the reaction and getting a more obvious result, the voltage supplied by DC power is set higher than the minimum voltage requirement and 0.1 mol/L K_2SO_4 is added to the solution to acquire a larger current. It is clear that after 6 h of reaction, nitrate is effectively degraded by the electrocatalytic system (Figure 3c).

Moreover, NO_3^- can be reduced into a series of substances.^{37,39,43,44} The relative reactions are as follows.



Therefore, another two byproducts, NO_2^- and NH_3 , are determined before and after reaction as well (Figure 3d,e), and

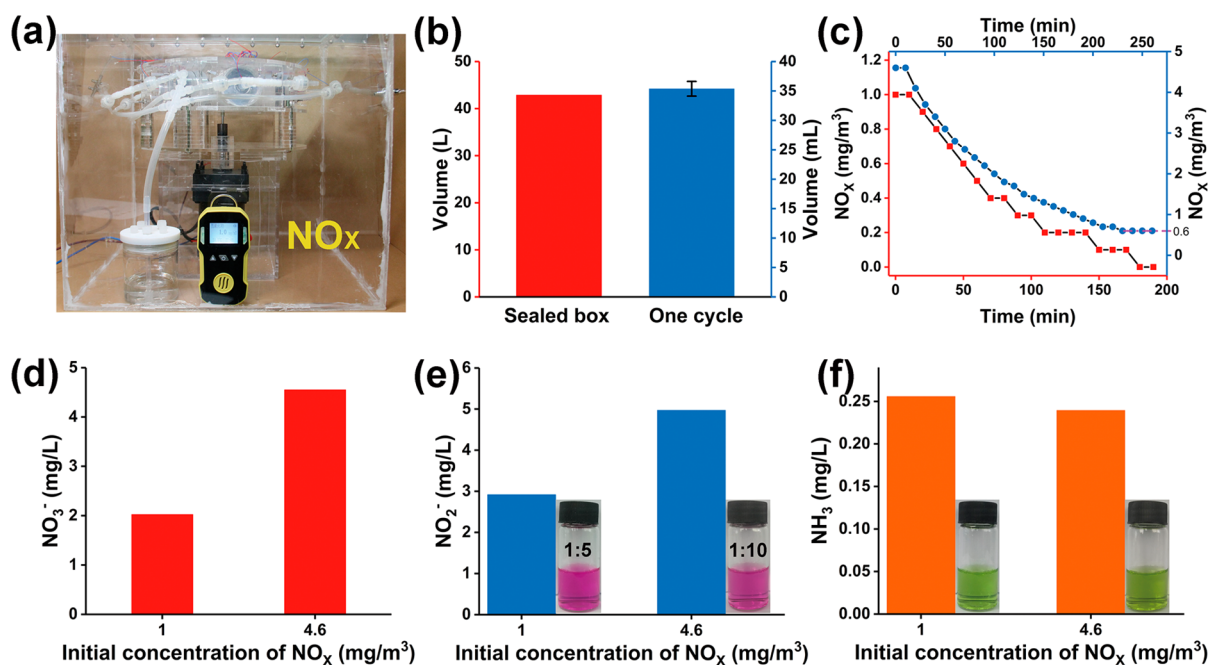


Figure 5. Absorption of NO_x . (a) Photograph of the sealed box with electrolytic cell, NO_x detector, and the radial-engine-shaped TENGs driven by a motor. (b) Volume of the sealed box and air by one circle rotation with the radial-engine-shaped TENGs. (c) Concentration variation of NO_x in the sealed box starting from 1.0 and 4.6 mg/m^3 separately. (d) Detection results of NO_3^- and (e) NO_2^- and (f) NH_3 in the water when the concentration of NO_x remained in the sealed box at a steady state.

their standard calibration curves are also made (Figure S6c–f). Through absorption curves and photographs, there are significant signs that NO_2^- and NH_3 are formed during the reaction. Since TENGs' output is easily affected by the external circuit condition and the electrocatalytic reaction needs enough applied voltage, a series of concentrations of NO_3^- solutions are prepared as electrolytes. At the rotation frequency of 3 Hz, the voltage between two electrodes and the current are tested. As shown in Figure 3f, the voltage decreases significantly accompanied by the increase in NO_3^- concentration. Meanwhile, there is no obvious change in the peak current, as shown in Figure 3g. Based on the above, a concentration of 1 mg/L NO_3^- is chosen as the primary solution. After 6 h of reaction, nitrate is degraded with a distinguishable change in the absorption curve under the drive of radial-engine-shaped TENGs (Figure 3h). Although no determination data show the product of NO_2^- , the slight change from the photograph and absorption curve for NH_3 generation could not be neglected (Figure 3i).

As for the degradation of nitrite, the CV curve is measured in 1 mg/L NO_2^- solution with the reference of SCE (Figure 4a).^{39,44} In the simulation degradation experiments, 0.2 mg/L NO_2^- is used as pollutant source containing 0.1 mol/L K_2SO_4 . Similarly, driven by a DC power at -3 V, nitrite can be effectively degraded after 6 h of electrocatalytic reaction (Figure 4b), and the degradation product NH_3 is detected as well (Figure 4c). The concentration change is minor and just above the acceptable determination limit. It is important to note that the oxidation reaction on the anode is carried out simultaneously. Although the concentration change is not detected (Figure S7), NO_2^- could be oxidized back to NO_3^- again. Driven by the radial-engine-shaped TENGs at the rotation frequency of 3 Hz, the voltage and the current are tested using a series of increasing concentrations of NO_2^- solutions. As shown in Figure 4d and e, a significant drop and

tiny variations are observed at voltage and peak current, respectively. The following TENGs-driven degradation experiment with 0.1 mg/L NO_2^- shows that NO_2^- is degraded effectively (Figure 4f). Besides, no distinguishing concentration variations of NO_3^- and NH_3 are identified.

To verify the practicability of air flow control by one-way valves and the absorption of NO_x , a simulation experiment is conducted in a sealed box. Figure 5a shows a photograph of the setup, in which the radial-engine-shaped TENGs with one-way valves, power source, electrolytic cell with 50 mL of pure water, and NO_x detector are sealed. All gas tubes are gathered through a six-way valve and connected to the electrolytic cell. The volume data of sealed box and one circle rotation transported gas measured by the drainage method are shown in Figure 5b. By the chemical reaction between the Cu sheet and concentrated nitric acid, the pollution source is acquired. Since the quantity and the form of NO_x are not easy to control during reaction, an excess amount of pollutant is allowed into the box first. With the help of a micro air pump, the concentration of NO_x is adjusted to 1.0 and 4.6 mg/m^3 as initial value separately in two independent experiments. After the concentration is steady for 10 min, the motor starts running and the detector value is recorded every 10 min until the concentration comes to a rebuilt steady state. For the initial concentration of 1.0 mg/m^3 , no NO_x is detected after 170 min of absorption. For a higher concentration at 4.6 mg/m^3 , the final concentration stabilized at 0.6 mg/m^3 for more than half an hour. It is inferred that the substances in the aqueous solution reach saturation. Then the concentrations of NO_3^- and NO_2^- are determined to see the degree of absorption (Figure 5d,e). It must be noted that the determination limit of NO_2^- is exceeded in both solutions. Thus, the solutions are diluted in the ratios of 1:5 and 1:10 to be measured, and then the calculated data from the absorption curve are multiplied by corresponding dilution factor. In addition, NH_3 is also detected

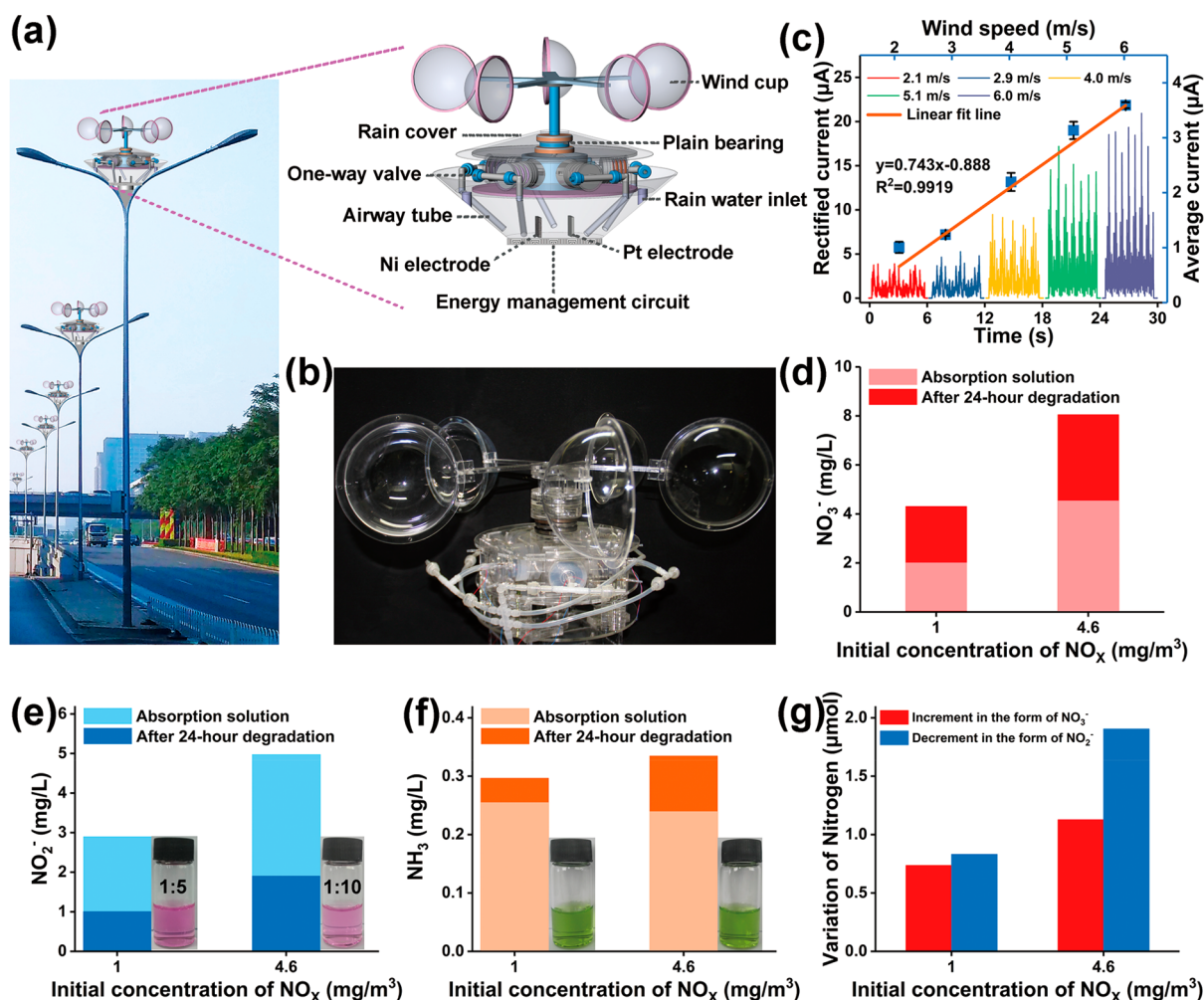


Figure 6. Self-powered NO_x degradation by the radial-engine-shaped TENGs. (a) Schematic diagram of the self-powered radial-engine-shaped TENG system driven by wind power. (b) Photograph of the self-powered radial-engine-shaped TENGs. (c) Rectified short-circuit current at different wind speeds and the linear relation between average current and wind speed. (d) Detection results of NO_3^- and (e) NO_2^- and (f) NH_3 after 24-h of self-powered degradation using a 20 mL absorption solution from the simulation absorption experiment. (g) Variation of nitrogen in moles from NO_3^- and NO_2^- .

because of the possibility of the existence of ammonia in air,⁴⁵ and Figure 5f shows the results.

Based on all of the above, it is indicated that the absorption and electrocatalytic degradation system could work well driven by the radial-engine-shaped TENGs. Subsequently, we demonstrated it could be a self-powered system under blowing wind. As shown in Figure 6a, after integrated with wind cups, the whole device can be set on high objects such as a street light pole to solve the NO_x pollution problem by wind. Besides, a plain bearing is used to keep the rotational stability. Furthermore, by using rain cover and rainwater management, the system could have the maximum utilization of natural resources. Figure 6b is a photograph of the real device after the wind cup is installed. An electric fan is used to supply artificial wind. Due to the uneven wind, the measured speed data with multipoint statistics are illustrated in Figure S8. Figure 6c shows the rectified peak current and the linear relation between the average current and wind speed. Both peak current and average current increase as the wind speeds up. The video in the Supporting Information is a demo of the self-powered NO_x absorption and degradation system driven by wind.

A 20 mL absorption solution is transferred into the catalytic system and driven by the radial-engine-shaped TENGs at a wind speed of 6 m/s. After 24 h of reaction, NO_3^- , NO_2^- , and NH_3 are all determined (Figure 6d–f, Figure S9). It is interesting to note that the concentration of NO_3^- increases significantly instead of decreasing as expected. Meanwhile, the concentration values of NO_2^- show a notable decline. It is deduced that NO_2^- is oxidized on the anode surface. Due to its high concentration, the probability of contact and reaction with the electrode increases. After calculation, the increased quantity in moles of NO_3^- is less than the decreased moles of NO_2^- (Figure 6g). Therefore, the pollutants are really continuously self-powered degraded by the radial-engine-shaped TENGs with wind power. Moreover, the concentration increase of NH_3 also explains the occurrence of effective degradation reaction.

CONCLUSIONS

In conclusion, a self-powered NO_x absorption and degradation system was constructed, by employing the radial-engine-shaped TENGs, one-way valves, and a Ni–Pt electrocatalytic system. Due to the characteristics of phase position, the radial-

engine-shaped TENGs output a continuous DC current after rectification. KNO_3 and KNO_2 are used as the simulated pollution source, and the catalytic system works well on the degradation by both DC source simulation and the radial-engine-shaped TENGs. Moreover, in a sealed simulation environment, the NO_x generated by a chemical method is well absorbed in the water. Finally, the above solution was effectively degraded by our system under an artificial wind of 6 m/s. Compared with the traditional pressurization and catalytic reduction methods, the self-powered system possesses advantages of low cost, simple materials, and low equipment requirements. It could serve as disturbed NO_x cleaners without any power supply. In addition, the simultaneous realization of absorption and degradation in aqueous solution by wind makes it a better fit for trace NO_x in the open environment and an important complement to traditional methods. This work also provides an approach for the removal of polluted gas in our environment using a self-powered electrochemical system.

METHODS

Fabrication of the Stacked TENGs. The substrate of the PET film (0.45 mm) was cut by a laser cutting machine into a shape with 9 circular units as shown in Figure S1 (i). The diameter of the circular unit is 47.5 mm. Then the buffer layer of black sponge discs with a diameter of 45 mm and thickness of 0.5 mm is stuck to both sides of the PET except two end units to one side. With the use of small through-holes of the PET, short wires are used for the connection of Cu electrodes (30 μm) on the sponge. Last, the dielectric material PTFE film (80 μm) is stuck on the Cu electrode alternately at both sides to fabricate the stacked TENGs.

Fabrication and Measurements of the Radial-Engine-Shaped TENGs. As shown in Figure S2b, the key actuating device is made first. Then the actuating shaft of device is fitted with the bearing in a PMMA disc base with a diameter of 25 cm. The chamber for the piston is cut from a syringe that is made from PP. The length of the chamber is 6 cm, and the inner diameter is 50 mm. After five chambers are matched to pistons and fixed with a PMMA frame on the disc base, another PMMA disc is put on the top of the chambers. Meanwhile, five position control baffles are set at the end of the chambers to tune the position of the chambers and fit the piston movements. The successfully fabricated radial-engine-shaped TENG system is connected to a DC electric motor (07SC, GPG Ltd.). All basic performance data are measured by an electrometer (6514, Keithley Ltd.) with the LabVIEW program. The average current data are calculated from the rectified current by the integration function of Origin software. The average power data are based on the average current with a series of external resistances. For the charging performance, each capacitor is discharged to zero before the test. Since NO_x is a kind of corrosive gas, a simple stability experiment is conducted as well (Figure S10), and more details are illustrated in the Supporting Information.

Degradation of NO_3^- and NO_2^- . The electrocatalytic system is composed of Ni foam as a working electrode and Pt as a counter electrode. Ni foam is 1.5 mm thick, and the pore diameter is 0.2 to 0.6 mm. Both electrodes have a size of 1 cm^2 square, and the distance between them is 2 cm. KNO_3 and KNO_2 are used as simulated pollutants in the solution. Before the degradation experiments, the CV curves are tested at a scan rate of 5 mV/s from 0 to -1.5 V using 20 mL of 10 mg/L NO_3^- and 1 mg/L NO_2^- by an electrochemical workstation (CHI 660E, CHEN HUA Ltd.). A 20 mL amount of 20 mg/L NO_3^- and 0.2 mg/L NO_2^- both with 0.1 mol/L K_2SO_4 are used as electrolyte separately and degraded under -3 V by DC power. When the reaction is driven by the radial-engine-shaped TENGs, the rotation frequency is set at 3 Hz by controlling the motor. Ultraviolet or visible light absorption spectrometry is used for determining the concentration of NO_3^- , NO_2^- , and NH_3 . For more details about determination, please see the Supporting Information.

Self-Powered Degradation of the Absorption Solutions.

Disconnected from the motor, the radial-engine-shaped TENGs are turned over and fixed again on the PMMA base. Then a paddle with five wind cups is installed on the actuating shaft to harvest wind energy for self-powered degradation. The diameters of the paddle and wind cup are 64 and 15 cm, respectively. By an electric fan, artificial wind of 6 m/s drives the radial-engine-shaped TENGs with an electrocatalytic system for 24 h to degrade 20 mL of the absorption solution from the NO_x absorption simulation experiments.

ASSOCIATED CONTENT

Supporting Information

The Supporting Information is available free of charge at <https://pubs.acs.org/doi/10.1021/acsnano.9b08496>.

Chemicals, determination details, and additional figures: schematic diagram of the absorption and degradation process, fabrication of the key actuating device and the stacked TENGs, photograph of the top view of the radial-engine-shaped TENGs with an air flow control device, multiples of average current and power comparison, standard calibration curves, a typical UV-vis absorption curve of NO_3^- in the NO_2^- degradation experiment, corresponding relation between measured and preset wind speed, UV-vis absorption curves of NO_3^- , NO_2^- , and NH_3 by self-powered degradation, stability experiment (PDF)

Video of the self-powered NO_x absorption and degradation system driven by wind (MP4)

AUTHOR INFORMATION

Corresponding Authors

Wei Tang – CAS Center for Excellence in Nanoscience, Beijing Institute of Nanoenergy and Nanosystems, Chinese Academy of Sciences, Beijing 100083, People's Republic of China; Center on Nanoenergy Research, School of Physical Science and Technology, Guangxi University, Nanning 530004, People's Republic of China; Email: tangwei@binn.cas.cn

Zhong Lin Wang – CAS Center for Excellence in Nanoscience, Beijing Institute of Nanoenergy and Nanosystems, Chinese Academy of Sciences, Beijing 100083, People's Republic of China; School of Nanoscience and Technology, University of Chinese Academy of Sciences, Beijing 100049, People's Republic of China; Center on Nanoenergy Research, School of Physical Science and Technology, Guangxi University, Nanning 530004, People's Republic of China; School of Material Science and Engineering, Georgia Institute of Technology, Atlanta, Georgia 30332-0245, United States; orcid.org/0000-0002-5530-0380; Email: zlwang@gatech.edu

Authors

Kai Han – CAS Center for Excellence in Nanoscience, Beijing Institute of Nanoenergy and Nanosystems, Chinese Academy of Sciences, Beijing 100083, People's Republic of China; School of Nanoscience and Technology, University of Chinese Academy of Sciences, Beijing 100049, People's Republic of China

Jianjun Luo – CAS Center for Excellence in Nanoscience, Beijing Institute of Nanoenergy and Nanosystems, Chinese Academy of Sciences, Beijing 100083, People's Republic of China; School of Nanoscience and Technology, University of Chinese Academy of Sciences, Beijing 100049, People's Republic of China

Yawei Feng – CAS Center for Excellence in Nanoscience, Beijing Institute of Nanoenergy and Nanosystems, Chinese Academy of Sciences, Beijing 100083, People's Republic of China; School of

Nanoscience and Technology, University of Chinese Academy of Sciences, Beijing 100049, People's Republic of China

Qingsong Lai – CAS Center for Excellence in Nanoscience, Beijing Institute of Nanoenergy and Nanosystems, Chinese Academy of Sciences, Beijing 100083, People's Republic of China; School of Nanoscience and Technology, University of Chinese Academy of Sciences, Beijing 100049, People's Republic of China

Yu Bai – CAS Center for Excellence in Nanoscience, Beijing Institute of Nanoenergy and Nanosystems, Chinese Academy of Sciences, Beijing 100083, People's Republic of China; School of Nanoscience and Technology, University of Chinese Academy of Sciences, Beijing 100049, People's Republic of China

Complete contact information is available at:
<https://pubs.acs.org/10.1021/acsnano.9b08496>

Notes

The authors declare no competing financial interest.

ACKNOWLEDGMENTS

The research was supported by the National Key R & D Project from the Minister of Science and Technology (2016YFA0202704), Youth Innovation Promotion Association, CAS, Beijing Municipal Science & Technology Commission (Z171100000317001, Z171100002017017, Y3993113DF), and National Natural Science Foundation of China (Grant No. 51605033, 51432005, 5151101243, 51561145021).

REFERENCES

- (1) Lee, D. S.; Kohler, I.; Grobler, E.; Rohrer, F.; Sausen, R.; Gallardo-Klenner, L.; Olivier, J. G. J.; Dentener, F. J.; Bouwman, A. F. Estimations of Global NO_x Emissions and Their Uncertainties. *Atmos. Environ.* **1997**, *31*, 1735–1749.
- (2) Zhang, Q.; Streets, D. G.; Carmichael, G. R.; He, K. B.; Huo, H.; Kannari, A.; Klimont, Z.; Park, I. S.; Reddy, S.; Fu, J. S.; Chen, D.; Duan, L.; Lei, Y.; Wang, L. T.; Yao, Z. L. Asian Emissions in 2006 for the NASA INTEX-B Mission. *Atmos. Chem. Phys.* **2009**, *9*, 5131–5153.
- (3) Bilgen, S. Structure and Environmental Impact of Global Energy Consumption. *Renewable Sustainable Energy Rev.* **2014**, *38*, 890–902.
- (4) Shindell, D.; Smith, C. J. Climate and Air-Quality Benefits of a Realistic Phase-Out of Fossil Fuels. *Nature* **2019**, *573*, 408–411.
- (5) Skalska, K.; Miller, J. S.; Ledakowicz, S. Trends in NO_x Abatement: A Review. *Sci. Total Environ.* **2010**, *408*, 3976–3989.
- (6) Xalxo, R.; Sahu, K. Acid Rain-Induced Oxidative Stress Regulated Metabolic Interventions and Their Amelioration Mechanisms in Plants. *Biologia* **2017**, *72*, 1387–1393.
- (7) Chestnut, L. G.; Mills, D. M. A Fresh Look at the Benefits and Costs of the US Acid Rain Program. *J. Environ. Manage.* **2005**, *77*, 252–266.
- (8) Bascom, R.; Bromberg, P. A.; Costa, D. A.; Devlin, R.; Dockery, D. W.; Frampton, M. W.; Lambert, W.; Samet, J. M.; Speizer, F. E.; Utell, M. Health Effects of Outdoor Air Pollution. *Am. J. Respir. Crit. Care Med.* **1996**, *153*, 3–50.
- (9) Kampa, M.; Castanas, E. Human Health Effects of Air Pollution. *Environ. Pollut.* **2008**, *151*, 362–367.
- (10) Pénard-Morand, C.; Raherison, C.; Charpin, D.; Kopferschmitt, C.; Lavaud, F.; Caillaud, D.; Annesi-Maesano, I. Long-Term Exposure to Close-Proximity Air Pollution and Asthma and Allergies in Urban Children. *Eur. Respir. J.* **2010**, *36*, 33–40.
- (11) Gehring, U.; Gruzieva, O.; Agius, R. M.; Beelen, R.; Custovic, A.; Cyrys, J.; Eeftens, M.; Flexeder, C.; Fuertes, E.; Heinrich, J.; Hoffmann, B.; de Jongste, J. C.; Kerkhof, M.; Klümper, C.; Korek, M.; Mölter, A.; Schultz, E. S.; Simpson, A.; Sugiri, D.; Svartengren, M.; et al. Air Pollution Exposure and Lung Function in Children: The ESCAPE Project. *Environ. Health Perspect.* **2013**, *121*, 1357–1364.
- (12) Busca, G.; Lietti, L.; Ramis, G.; Berti, F. Chemical and Mechanistic Aspects of the Selective Catalytic Reduction of NO_x by Ammonia over Oxide Catalysts: A Review. *Appl. Catal., B* **1998**, *18*, 1–36.
- (13) Sullivan, J. A.; Doherty, J. A. NH₃ and Urea in the Selective Catalytic Reduction of NO_x over Oxide-Supported Copper Catalysts. *Appl. Catal., B* **2005**, *55*, 185–194.
- (14) Roy, S.; Hegde, M. S.; Madras, G. Catalysis for NO_x Abatement. *Appl. Energy* **2009**, *86*, 2283–2297.
- (15) Twigg, M. V. Catalytic Control of Emissions from Cars. *Catal. Today* **2011**, *163*, 33–41.
- (16) Lee, Y.-N.; Schwartz, S. E. Reaction Kinetics of Nitrogen Dioxide with Liquid Water at Low Partial Pressure. *J. Phys. Chem.* **1981**, *85*, 840–848.
- (17) Ting, T.; Stanger, R.; Wall, T. Laboratory Investigation of High Pressure NO Oxidation to NO₂ and Capture with Liquid and Gaseous Water under Oxy-Fuel CO₂ Compression Conditions. *Int. J. Greenhouse Gas Control* **2013**, *18*, 15–22.
- (18) Li, J.; Han, X.; Zhang, X.; Sheveleva, A. M.; Cheng, Y.; Tuna, F.; McInnes, E. J. L.; McCormick McPherson, L. J.; Teat, S. J.; Daemen, L. L.; Ramirez-Cuesta, A. J.; Schröder, M.; Yang, S. Capture of Nitrogen Dioxide and Conversion to Nitric Acid in a Porous Metal-Organic Framework. *Nat. Chem.* **2019**, *11*, 1085–1090.
- (19) Fan, F.-R.; Tian, Z.-Q.; Wang, Z. L. Flexible Triboelectric Generator! *Nano Energy* **2012**, *1*, 328–334.
- (20) Wang, Z. L. On Maxwell's Displacement Current for Energy and Sensors: The Origin of Nanogenerators. *Mater. Today* **2017**, *20*, 74–82.
- (21) Niu, S.; Wang, Z. L. Theoretical Systems of Triboelectric Nanogenerators. *Nano Energy* **2015**, *14*, 161–192.
- (22) Wang, Z. L. Triboelectric Nanogenerators as New Energy Technology for Self-Powered Systems and as Active Mechanical and Chemical Sensors. *ACS Nano* **2013**, *7*, 9533–9557.
- (23) Tang, W.; Zhang, C.; Han, C. B.; Wang, Z. L. Enhancing Output Power of Cylindrical Triboelectric Nanogenerators by Segmentation Design and Multilayer Integration. *Adv. Funct. Mater.* **2014**, *24*, 6684–6690.
- (24) Zhu, G.; Bai, P.; Chen, J.; Jing, Q.; Wang, Z. L. Triboelectric Nanogenerators as a New Energy Technology: From Fundamentals, Devices, to Applications. *Nano Energy* **2015**, *14*, 126–138.
- (25) Tang, W.; Jiang, T.; Fan, F. R.; Yu, A. F.; Zhang, C.; Cao, X.; Wang, Z. L. Liquid-Metal Electrode for High-Performance Triboelectric Nanogenerator at an Instantaneous Energy Conversion Efficiency of 70.6%. *Adv. Funct. Mater.* **2015**, *25*, 3718–3725.
- (26) Fan, F. R.; Tang, W.; Wang, Z. L. Flexible Nanogenerators for Energy Harvesting and Self-Powered Electronics. *Adv. Mater.* **2016**, *28*, 4283–4305.
- (27) Wang, Z. L.; Jiang, T.; Xu, L. Toward the Blue Energy Dream by Triboelectric Nanogenerator Networks. *Nano Energy* **2017**, *39*, 9–23.
- (28) Ma, M.; Kang, Z.; Liao, Q.; Zhang, Q.; Gao, F.; Zhao, X.; Zhang, Z.; Zhang, Y. Development, Applications, and Future Directions of Triboelectric Nanogenerators. *Nano Res.* **2018**, *11*, 2951–2969.
- (29) Zhang, X.-S.; Han, M.; Kim, B.; Bao, J.-F.; Brugger, J.; Zhang, H. All-in-One Self-Powered Flexible Microsystems Based on Triboelectric Nanogenerators. *Nano Energy* **2018**, *47*, 410–426.
- (30) Wu, C.; Wang, A. C.; Ding, W.; Guo, H.; Wang, Z. L. Triboelectric Nanogenerator: A Foundation of the Energy for the New Era. *Adv. Energy Mater.* **2019**, *9*, 1802906.
- (31) Chen, B.; Yang, Y.; Wang, Z. L. Scavenging Wind Energy by Triboelectric Nanogenerators. *Adv. Energy Mater.* **2018**, *8*, 1702649.
- (32) Kim, D.; Tcho, I.-W.; Choi, Y.-K. Triboelectric Nanogenerator Based on Rolling Motion of Beads for Harvesting Wind Energy as Active Wind Speed Sensor. *Nano Energy* **2018**, *52*, 256–263.
- (33) Park, S.-J.; Lee, S.; Seol, M.-L.; Jeon, S.-B.; Bae, H.; Kim, D.; Cho, G.-H.; Choi, Y.-K. Self-Sustainable Wind Speed Sensor System with Omni-Directional Wind Based Triboelectric Generator. *Nano Energy* **2019**, *55*, 115–122.

(34) Zhu, H. R.; Tang, W.; Gao, C. Z.; Han, Y.; Li, T.; Cao, X.; Wang, Z. L. Self-Powered Metal Surface Anti-Corrosion Protection Using Energy Harvested from Rain Drops and Wind. *Nano Energy* **2015**, *14*, 193–200.

(35) Chen, S.; Gao, C.; Tang, W.; Zhu, H.; Han, Y.; Jiang, Q.; Li, T.; Cao, X.; Wang, Z. Self-Powered Cleaning of Air Pollution by Wind Driven Triboelectric Nanogenerator. *Nano Energy* **2015**, *14*, 217–225.

(36) Feng, Y.; Han, K.; Jiang, T.; Bian, Z.; Liang, X.; Cao, X.; Li, H.; Wang, Z. L. Self-Powered Electrochemical System by Combining Fenton Reaction and Active Chlorine Generation for Organic Contaminant Treatment. *Nano Res.* **2019**, *12*, 2729–2735.

(37) Duarte, H. A.; Jha, K.; Weidner, J. W. Electrochemical Reduction of Nitrates and Nitrites in Alkaline Media in the Presence of Hexavalent Chromium. *J. Appl. Electrochem.* **1998**, *28*, 811–817.

(38) Li, H.-L.; Robertson, D. H.; Chambers, J. Q.; Hobbs, D. T. Electrochemical Reduction of Nitrate and Nitrite in Concentrated Sodium Hydroxide at Platinum and Nickel Electrodes. *J. Electrochem. Soc.* **1998**, *135*, 1154–1158.

(39) Mattarozzi, L.; Cattarin, S.; Comisso, N.; Guerriero, P.; Musiani, M.; Vázquez-Gómez, L.; Verlato, E. Electrochemical Reduction of Nitrate and Nitrite in Alkaline Media at CuNi Alloy Electrodes. *Electrochim. Acta* **2013**, *89*, 488–496.

(40) Reyter, D.; Bélanger, D.; Roué, L. Optimization of the Cathode Material for Nitrate Removal by a Paired Electrolysis Process. *J. Hazard. Mater.* **2011**, *192*, 507–513.

(41) Ryu, H.; Lee, J. H.; Khan, U.; Kwak, S. S.; Hinchet, R.; Kim, S.-W. Sustainable Direct Current Powering Triboelectric Nanogenerator via Intent Asymmetrical Design. *Energy Environ. Sci.* **2018**, *11*, 2057–2063.

(42) Kim, T.; Kim, D. Y.; Yun, J.; Kim, B.; Lee, S. H.; Kim, D.; Lee, S. Direct-Current Triboelectric Nanogenerator via Water Electrification and Phase Control. *Nano Energy* **2018**, *52*, 95–104.

(43) Bouzek, K.; Paidar, M.; Sadilkova, A.; Bergmann, H. Electrochemical Reduction of Nitrate in Weakly Alkaline Solutions. *J. Appl. Electrochem.* **2001**, *31*, 1185–1193.

(44) Sahin, A.; Lin, W.-T.; Khunjar, W. O.; Chandran, K.; Banta, S.; West, A. C. Electrochemical Reduction of Nitrite to Ammonia for Use in a Bioreactor. *J. Electrochem. Soc.* **2013**, *160*, G19–G26.

(45) Daioglou, V.; Faaij, A. P. C.; Saygin, D.; Patel, M. K.; Wicke, B.; van Vuuren, D. P. Energy Demand and Emissions of the Non-Energy Sector. *Energy Environ. Sci.* **2014**, *7*, 482–498.